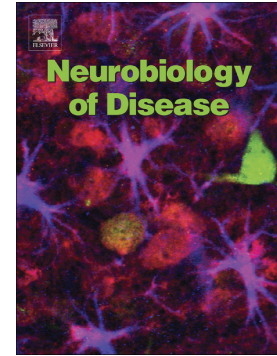# Journal Pre-proof

Quantifying local field potential dynamics with amplitude and frequency stability between ON and OFF medication and stimulation in Parkinson's disease

Xuanjun Guo, Shenghong He, Xinyi Geng, Pan Yao, Christoph Wiest, Yingnan Nie, Huiling Tan, Shouyan Wang

Please cite this article as: X. Guo, S. He, X. Geng, et al., Quantifying local field potential dynamics with amplitude and frequency stability between ON and OFF medication and stimulation in Parkinson's disease, *Neurobiology of Disease* (2023), https://doi.org/10.1016/j.nbd.2024.106519

This is a PDF file of an article that has undergone enhancements after acceptance, such as the addition of a cover page and metadata, and formatting for readability, but it is not yet the definitive version of record. This version will undergo additional copyediting, typesetting and review before it is published in its final form, but we are providing this version to give early visibility of the article. Please note that, during the production process, errors may be discovered which could affect the content, and all legal disclaimers that apply to the journal pertain.

Quantifying local field potential dynamics with amplitude and frequency stability between ON and OFF medication and stimulation in Parkinson's disease

Xuanjun Guo[1,2,3,4,5], Shenghong He[2], Xinyi Geng[1], Pan Yao[2,8,9], Christoph Wiest[2], Yingnan Nie[1,3,4,5], Huiling Tan[2], Shouyan Wang[1,3,4,5,6]

Affiliations:

1. Institute of Science and Technology for Brain-Inspired Intelligence, Fudan University, Shanghai, China;
2. Medical Research Council Brain Network Dynamics Unit, Nuffield Department of Clinical Neurosciences, University of Oxford, Oxford, United Kingdom;
3. Key Laboratory of Computational Neuroscience and Brain-Inspired Intelligence (Fudan University), Ministry of Education, China;
4. MOE Frontiers Center for Brain Science, Fudan University, Shanghai, China;
5. Zhangjiang Fudan International Innovation Center, Shanghai, China;
6. Shanghai Engineering Research Center of AI & Robotics, Fudan University, Shanghai, China;
7. Engineering Research Center of AI & Robotics, Ministry of Education, Fudan University, Shanghai, China;
8. State Key Laboratory of Transducer Technology, Aerospace Information Research Institute (AIR), Chinese Academy of Sciences, 100094 Beijing, China;
9. School of Electronic, Electrical, and Communication Engineering, University of Chinese Academy of Sciences (UCAS), 100049 Beijing, China.

Send correspondence to:

Shouyan Wang: shouyan@fudan.edu.cn;
Huiling Tan: huiling.tan@ndcn.ox.ac.uk.

Abstract

Neural oscillations are critical to understanding the synchronisation of neural activities and their relevance to neurological disorders. For instance, the amplitude of beta oscillations in the subthalamic nucleus has gained extensive attention, as it has been found to correlate with medication status and the therapeutic effects of continuous deep brain stimulation in people with Parkinson's disease. However, the frequency stability of subthalamic nucleus beta oscillations, which has been suggested to be associated with dopaminergic information in brain states, has not been well explored. Moreover, the administration of medicine can have inverse effects on changes in frequency and amplitude. In this study, we proposed a method based on the stationary wavelet transform to quantify the amplitude and frequency stability of subthalamic nucleus beta oscillations and evaluated the method using simulation and real data for Parkinson's disease patients. The results suggest that the amplitude and frequency stability quantification has enhanced sensitivity in distinguishing pathological conditions in Parkinson's disease patients. Our quantification shows the benefit of combining frequency stability information with amplitude and provides a new potential feedback signal for adaptive deep brain stimulation.

Keywords

Contributions of authors

Xuanjun Guo: Methodology, Formal analysis, Investigation, Writing—Original Draft
Shenghong He: Validation, Investigation, Writing—Review & Editing
Xinyi Geng: Methodology, Writing—Review & Editing
Pan Yao: Investigation, Writing—Review & Editing
Christoph Wiest, Yingnan Nie: Data Curation
Huiling Tan: Validation, Investigation, Writing—Review & Editing
Shouyan Wang: Methodology, Formal analysis, Writing—Original Draft

Data accessibility

Data analysed in this study are already shared on the MRC Brain Network Dynamics Unit data sharing platform: https://data.mrc.ox.ac.uk/stn-lfp-on-off-and-dbs.

Introduction

Local field potentials (LFPs) recorded in the nuclei of basal ganglia serve as indicators of synchronous changes in large populations of neurons at the mesoscopic scale [1]–[5]. In Parkinson's disease (PD) patients, exaggerated neural synchronisation has been found in the basal ganglia, indicating elevated power in the LFPs over beta frequencies, especially in the low-beta band (12–24 Hz) [1]. An increase in beta-band (8–35 Hz) power has primarily been related to bradykinetic and rigid symptoms in the dopamine-depleted condition [5], [6], whereas the peak frequency of beta activity (usually around 20 Hz) has been found to correlate with the total score in part III (movement assessment) of the Unified Parkinson's Disease Ratings Scale (UPDRS) [7].

Given the correlation of beta oscillations with the severity of symptoms in PD, the instantaneous amplitude (IA; Fig. 1A) has been widely discussed. Previous studies have indicated that features extracted from oscillations around the peak frequency of beta activity (e.g., beta bursts [8], [9]) are good pathological markers of PD [8]–[11] because of their characteristic relations to the severity of symptoms. Beta power has been calculated online and used as a feedback signal in adaptive deep brain stimulation (DBS) [12]–[15]. In the online estimation of beta power, the peak beta frequency is often first quantified. The recorded LFPs are then band-pass filtered around the peak beta frequency [11], [12], and the amplitude of the envelope of the filtered signal (Amplitude; Fig. 1B) is extracted.

However, the amplitudes of peak beta oscillations are dynamic features that vary with time. These variations may result from fluctuations in the degree of synchronisation or the drift of the peak frequency. Unfortunately, the average power of a fixed frequency band does not reflect the drift of the peak frequency, and variations in the peak frequency have been considered as changes in synchronisation, which leads to a misunderstanding of the electrophysiological mechanism [5], [16]. In addition, some patients do not have a singular peak beta frequency but rather multiple peaks, which poses a challenge to real-time application [16], [17].

Although the instantaneous amplitude and instantaneous frequency (IF; Fig. 1A) obtained through an offline Hilbert transform both have important associations with the pathological mechanisms of PD [4], amplitude and frequency information might reflect interacting but different neuronal synchronisation activities of the subthalamic nucleus (STN) [4], [18]. Discontinuities in the instantaneous frequency [21], referred to as phase slips, do not correlate with corresponding instantaneous amplitude but rather are affected by dopaminergic conditions [4]. This indicates that neural synchronisation activity manifests not only in amplitude changes but also in frequency changes in the absence of amplitude changes. We thus hypothesise that a joint indicator is needed to make an appropriate measurement of brain oscillatory activity in PD.

In this paper, we propose an amplitude and frequency stability (AFS) quantification (AFS; Fig. 1B) based on stationary wavelet coefficients. The wavelet approach utilises a convolution process to generate coefficients such that it is sensitive to both amplitude and frequency stability. In contrast with the continuous wavelet transform, which is often used in offline analysis, the stationary wavelet transform (SWT) [19] is designed for online implementation and can retain time invariance during transformation. The adoption of the SWT thus improves the performance

of the method using the amplitude based on band-pass filtering (Amplitude; Fig 1B), which is currently implemented in adaptive DBS. Furthermore, compared with the adoption of the frequency stability (FS) based on band-pass filtering (FS; Fig 1B), the results are improved.

As the amplitude and FS are not correlated all the time, the objective of our work is to provide a quantification (i.e., the AFS) for considering amplitude changes and additional FS information in neural signals. We evaluate the correlation between the AFS and motor symptoms in PD. In the present study, the quantification of AFS was first illustrated using simulated signals derived from actual recordings and then applied to actual signals to assess how AFS in STN LFPs varied across various brain conditions (ON vs OFF dopaminergic medication and ON vs. OFF stimulation). In addition, we showed that the ability of AFS to reflect pathological information is insensitive to peak frequency drifts. Furthermore, we examined the importance of including FS in the context of PD and introduced a novel potential feedback signal for adaptive DBS.

Materials and Methods

Neural recordings of Parkinson's disease
In total, 34 PD patients (58 hemispheres) were included in this study. Local filed potential signals were recorded for 17 patients (32 hemispheres) in both ON and OFF dopaminergic medication statuses and for 17 PD patients (26 hemispheres) in both ON and OFF DBS statuses (130-Hz continuous stimulation). All of the patients provided informed consent, and the study was approved by local ethics committees.

ON/OFF medication recordings
Bipolar LFPs of STNs were recorded in 17 patients (four females) with advanced PD who underwent the bilateral implantation of DBS electrodes for clinical treatment before and after taking levodopa. The patients were 56.33 ± 6.872 years old. The subthalamic LFPs were recorded during an observation period after electrode implantation and before the implantation of an implantable pulse generator. The clinical details of the patients are summarised in Table 1. In addition, preoperative UPDRS Part III scores were obtained. All of the data were previously published in ref. [20] for patients 1–10 and in ref. [21] for patients 11–17.

ON/OFF DBS recordings
ON/OFF DBS recordings were collected for 17 patients (60.28 ± 5.727 years old, five females) who had DBS electrodes implanted in the STN. The clinical details of the patients are summarised in Table 1. In addition, preoperative UPDRS Part III scores were recorded for patients in OFF/ON medication states. All of the data of all patients were previously published in refs. [22]–[24].

Signal preprocessing
All recordings underwent the same preprocessing. Artefacts, including large baseline shifts and muscle movement artefacts, were rejected through visual inspection. Subsequently, segments with no apparent artefacts were selected for further analysis. For each recording, there was a segment of the raw signal having a minimum length of 100 s. The recordings were then filtered through a low-pass filter at 90 Hz and a high-pass filter at 2 Hz and resampled at 384 Hz to ensure that the decomposition frequency band met the requirement of the SWT. The new

sampling frequency was chosen such that the low-beta oscillations were situated in the fourth layer of stationary wavelet coefficients. Although the present study primarily focused on the low-beta band, other oscillations were also examined. The bands of the sixth, fifth, third, and second layers of stationary wavelet coefficients respectively corresponded to the theta (3–6 Hz), alpha (6–12 Hz), high-beta and low-gamma (24–48 Hz), and high-gamma (48–96 Hz) frequency bands of brain oscillations. An adaptive notch filter centred at 50 Hz was used to remove the line noise before the SWT. Channel selection on left and right side was based on previously published data, ensuring consistency in channel selection before and after treatment for each individual. All preprocessing procedures were implemented using the EEGLAB toolbox (version 2019.1) and customed scripts in MATLAB (version 9.8; MathWorks, Inc., Natick, MA, USA).

Table 1: Patient clinical details

ID	Gender	Age	DBS Target	Prep-op UPDRS III OFF (Med)	Prep-op UPDRS III ON (Med)
Med-1	M	58	Bilateral STN	47	15
Med-2	F	-	Bilateral STN	46	20
Med-3	M	60	Bilateral STN	42	25
Med-4	M	64	Bilateral STN	49	19
Med-5	M	60	Bilateral STN	37	10
Med-6	M	58	Bilateral STN	45	14
Med-7	F	60	Bilateral STN	37	12
Med-8	M	50	Bilateral STN	52	24
Med-9	M	65	Bilateral STN	23	7
Med-10	M	38	Bilateral STN	24	10
Med-11	M	57	Bilateral STN	54	14
Med-12	M	48	Bilateral STN	72	16
Med-13	F	58	Bilateral STN	56	16
Med-14	F	61	Bilateral STN	35	4
Med-15	M	54	Bilateral STN	53	19
Med-	M	58	Bilateral	43	25

16			STN		
Med-17	M	54	Bilateral STN	38	9
DBS-1	M	65	Bilateral STN	34	16
DBS-2	M	60	Left STN	50	30
DBS-3	F	63	Left STN	40	17
DBS-4	M	64	Right STN	52	21
DBS-5	M	53	Bilateral STN	23	12
DBS-6	M	54	Bilateral STN	51	35
DBS-7	M	58	Bilateral STN	41	16
DBS-8	M	60	Bilateral STN	31	4
DBS-9	F	64	Bilateral STN	29	6
DBS-10	M	63	Bilateral STN	51	27
DBS-11	M	47	Right STN	71	37
DBS-12	M	53	Right STN	38	25
DBS-13	F	69	Left STN	37	18.5
DBS-14	M	61	Left STN	24	12
DBS-15	M	61	Left STN	16	7
DBS-16	F	64	Left STN	26	13
DBS-17	F	66	Right STN	16	6

Prep-op: preoperative. UPDRS-III: Part III motor score on the Unified Parkinson's Disease Rating Scale. DBS: deep brain stimulation. Med: medication (levodopa).

Amplitude based on band-pass filtering

In the study of PD, the amplitudes of beta oscillations extracted using a band-pass filter (amplitude; Fig. 1B) have been widely investigated [8], [11], [12], [25]. We extracted the amplitudes of beta oscillations using a band-pass filter, adopting a method akin to that used in adaptive brain stimulation and burst analysis [11], [12]. Here, the amplitudes were extracted from the raw signal by correcting for the direct-current drift, then band-pass filtering followed by rectification, and finally smoothing with moving windows. The choice of the moving-window

length (600 ms) was analysed with the AFS quantification proposed in this study, with other window lengths also tested (as detailed later).

FS based on band-pass filtering

Similar to the extraction of amplitudes, the FS was determined by applying a band-pass filter to beta oscillations (FS; Fig 1B). FS is defined as the inverse of the standard deviation within a moving window of the instantaneous frequency obtained using a Hilbert transform. The window length (600 ms) was consistent with amplitude based on band-pass filtering.

Amplitude and frequency stability (AFS) quantification

The quantification (AFS; Fig 1B) methodology relies on the use of SWT. To estimate the quantification, a sliding window is applied to the stationary wavelet coefficients using the *minimax* criterion. This is a valuable means to represent the level of neural activity [26], [27], which can be simplified as the weighted standard deviation within the window [28]–[30]:

$$\hat{\sigma} \approx \frac{1}{0.6745} * Med(|W_{jk}|)$$

$$Thrs_{minimaxi} = \begin{cases} 0, N \leq 32 \\ 0.3936 + 0.1829 * \dfrac{Log_N}{Log_2}, N > 32 \end{cases}$$

$$AFS = \frac{\hat{\sigma} * Thrs_{minimaxi}}{\ln(j+1)}, j = 1, \ldots, L$$

where W_{jk} denotes stationary wavelet coefficients in the window, j denotes the decomposition layer (which corresponds to several frequency bands: theta (3-6 Hz), alpha (6-12 Hz), low-beta (12-24 Hz), high-beta and low-gamma (24-48 Hz), and high-gamma (48-96 Hz)) [31], and N is the number of samples in the window. As outlined in the previous section, the moving-window length (600 ms) was selected to achieve optimal performance in decoding the motor function. The results obtained in the testing of other lengths are presented in Supplementary Fig. 5. A comprehensive explanation of the calculation and implementation of the *minimax* criterion is presented in the Supplementary Materials (see Supplementary Fig. 1). The code has been published online: GuooooooXJ/AFSquantification: A method to jointly quantify amplitude and frequency stability information in neural signals (github.com).

The stationary wavelet method was adopted for the following reasons. The continuous wavelet transform is effective in characterising neuronal activity in offline analysis [8], [9], but it cannot be used in real time because it is non-causal. Although both the wavelet packet and discrete wavelet transform are causal, their coefficient lengths become progressively shorter upon the decomposition of layers [32]. In this context, the SWT compensates for the translation invariance lost in the discrete wavelet transform through down-sampling. The SWT is thus an appropriate choice for the quantification, as it may have the same length as the input signal in a real-time implementation setting [19], thus guaranteeing a more precise calculation of the standard deviation.

Evaluation of the distinguishability of pathophysiological oscillatory patterns

For each condition of interest (ON vs OFF medication, ON vs. OFF stimulation), we quantified the measures of synchrony (i.e., the amplitude, FS, and AFS) over time, and we used the Kullback–Leibler divergence (KLD) [33] between dynamic distributions to capture the distinguishability of different conditions. This statistical measure quantifies the dissimilarity between probability distributions of sequences and is formally defined by

$$D_{KL}(P||Q) = -\sum_{i \in X} P(i) ln \frac{Q(i)}{P(i)}$$

Here, $P(i)$ and $Q(i)$ are probabilities in the distribution of the i-th bin. In simulated signals, the distributions P and Q represent different amplitude and FS parameters for different simulation data. In real recordings, the distributions P and Q represent situations before and after treatment, respectively (Fig. 1C, OFF/ON medication). To compare the disparity between two conditions within one hemisphere, the same bin number (20) was used for the two histograms, and the bin size was accordingly calculated as

$$bin = \frac{Max - Min}{20}$$

where *Max* and *Min* encompass the entire range of the two conditions. This standardised approach ensures comparability across the specified conditions.

Generation and verification of simulated signals

Signal Generation

Simulated signals were obtained by adjusting the frequency component, amplitude, and phase of a real signal from case Med-16 in Table 1. Notably, the simulated signals in this study were focused within the low-beta band. The process, as illustrated in the Supplementary Materials (Supplementary Fig. 2), involved simulating signals by modifying two key parameters, namely the amplitude k and the standard deviation of the instantaneous frequency n [4], [34]. These manipulations allow for the systematic exploration and analysis of the effects of the amplitude and FS on the simulated signals within the target frequency band.

AFS, amplitude, and FS of the simulated signals

We performed two tests using a simulated signal with varying amplitude or FS. In comparing the ability of AFS quantification and the amplitude-based method to capture parameter changes, we generated two simulation signals having the same length (48 s). The two simulation signals were obtained from the same real signal, which was band-pass filtered over a low-beta band. We normalised the band-pass filtered signal in the range of [−1,1] to ensure that only the variable, either the amplitude or FS, was modified. The frequency-simulation signal had a FS n varying from 1 to 0.2, whereas the amplitude-simulation signal had an amplitude k varying from 1 to 5. We then used correlations between the indicators and corresponding parameter sequences (k or n) to assess the ability to capture amplitude or frequency information. Finally, the KLD was adopted to quantify the difference before and after parameter changes.
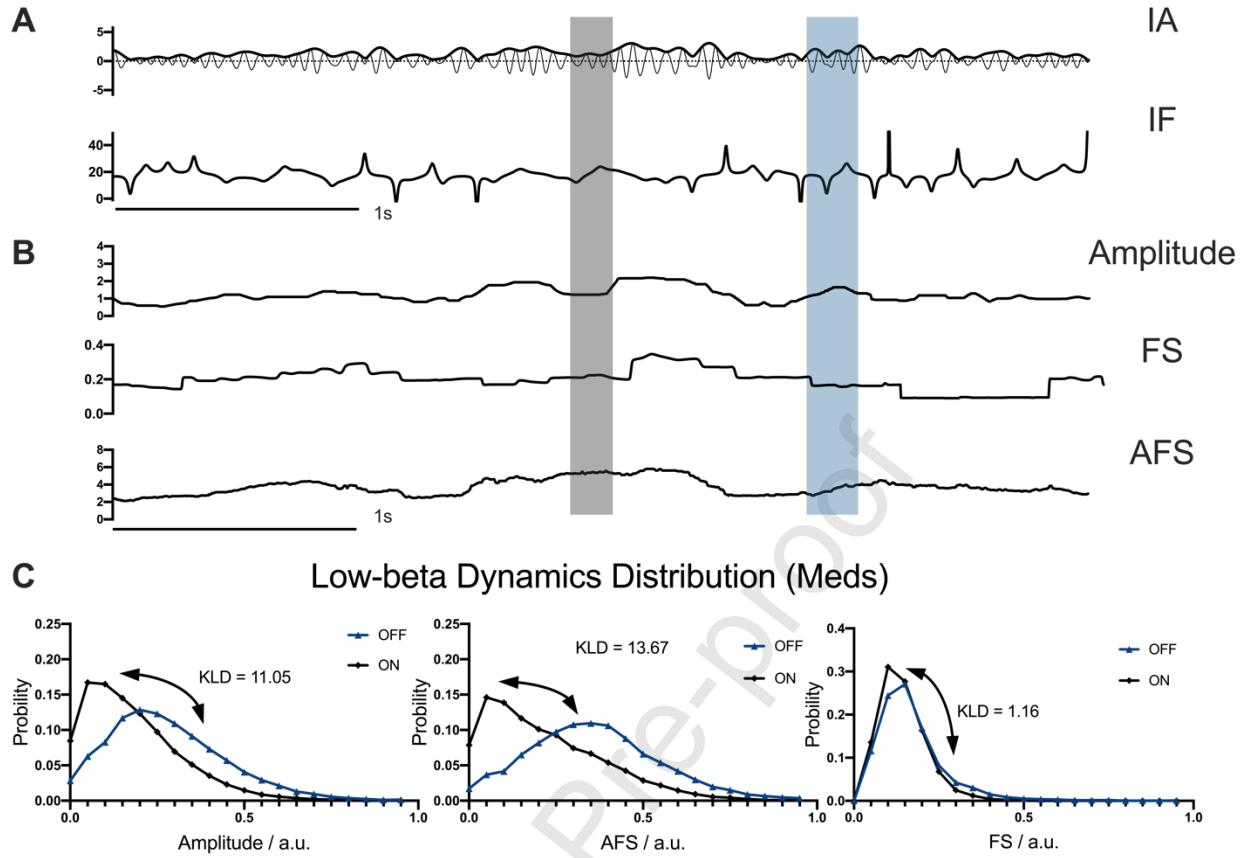
Figure 1: Amplitude and frequency stability (AFS) and amplitude or frequency stability (FS) based on band-pass filtering. (A) A segment of low-beta band filtered LFPs, in which the instantaneous amplitude (IA) and the instantaneous frequency (IF) obtained using an offline Hilbert transform are two independent measures of synchrony. (B) AFS, amplitude, and FS based on band-pass filtering at low beta. In a comparison of the grey area vs. the blue area, the amplitude based on band-pass filtering estimation method has a higher amplitude in the blue area than in the grey area; however, the AFS has the opposite result due to lower FS in the blue region. (C) KLD serving as a measurement of pairwise differences. The distributions of the dynamic amplitude based on band-pass filtering (left), AFS (middle), and FS (right) during ON/OFF medication conditions are presented, and the results are presented as an illustrative example of the visualisation of distributions averaged across all patients. To mitigate participant-based variations, all of the dynamics are normalised to the [0,1] range and are presented in units of hemisphere for visual representation. IA: instantaneous amplitude. IF: instantaneous frequency. AFS: amplitude and frequency stability. FS: frequency stability.

Comparisons of AFS under different conditions

After demonstrating the effects and sensitivity of the AFS quantification in identifying changes in amplitude and FS for simulated signals, we applied the quantification to real signals recorded under ON/OFF medication and ON/OFF stimulation to distinguish characteristics under different conditions. OFF medication data were recorded at least 12 hours after the withdrawal of medication, whereas OFF stimulation data were recorded 5 minutes after turning off DBS. Medication was not strictly controlled during the recording of ON/OFF stimulation, and the results are thus considered as the combined results of clinical treatment.

Distinguishing conditions using the broadband AFS and broadband amplitude or FS based on band-pass filtering

The AFS, amplitude, and FS based on band-pass filtering were calculated for STN LFPs from each hemisphere under conditions of ON/OFF levodopa medication and ON/OFF continuous 130-Hz DBS. We adopted the KLD to quantify the dissimilarity between two conditions. Continuous 36-s segments (corresponding to the shortest recording after preprocessing) were selected from all of the signals. In addition, by extending our analysis beyond the low-beta band, we made calculations on other frequency bands, namely the theta (3–6 Hz), alpha (6–12 Hz), high-beta and low-gamma (24–48 Hz), and high-gamma (48–96 Hz) bands. The results are presented in the Supplementary Fig 4. The selection of the window length presented a nuanced challenge. We thus tested various window lengths ranging from 0.3 to 1.4 s and chose the window length that provided the best performance in terms of decoding motor functions (i.e., 600 ms).

Distinguishing conditions using the broadband AFS and peak frequency power

As mentioned, the heterogeneity of the frequency distribution and dynamic drift of the peak frequency leads to errors in the estimation of power within a fixed frequency band. Previous studies have introduced the individualised peak frequency in calculating the beta power. To verify the adaptability of AFS quantification to drifts of the peak frequency, we compared the results calculated on segmented data and the whole data set for ON/OFF levodopa medication.

For the whole data set (having a duration of 36 s), the differences in the peak frequency of low-beta oscillation are defined as

$$Peak\ PSD_{Off-On} = \log(PSD_{peak}^{Off} - PSD_{peak}^{On})$$

Here, *PSD* refers to the power spectral density in the low-beta band. The peak frequency power was measured over the individually defined peak frequency and the adjacent bin on either side of the peak frequency (i.e., over a 5-Hz band) in OFF-med recordings. The same narrow band was used in the calculation of the peak frequency power for the ON-med recordings [7].

We hypothesise that the AFS is less sensitive to variations in the peak frequency, and therefore, the AFS is more robust in differentiating the effect of medication even on data in short time windows. To test this hypothesis, we randomly subsampled the low-beta bandpass filter signal 100 times, where each subsample comprised 3 s of data for each hemisphere in each medication condition. The peak frequency in all of the secondary segments was kept the same as that in the whole data set, and the peak power was measured as previously described but with a power spectral density for a period of 3 s. We then examined the correlations between medication-induced changes in the AFS or peak power with symptom alleviation for each subsample of data. The percentage of time in which the correlation was significant was quantified. As the time scale of a peak frequency drift may vary, other data lengths (i.e., 1, 2, and 4 s) were tested. In addition, considering that a shorter window length might be used for shorter segments, we tested window lengths ranging from 0.1 to 1.1 s and chose the length that had the highest proportion of significant correlations in the whole data set (250 ms).

Statistics

To investigate the effectiveness of the proposed quantification method in identifying changes in amplitude and FS, we examined the correlation between the parameter sequences of amplitude or FS and the corresponding mean values of the AFS quantification.

The AFS quantification was then applied to real neural recordings to further explore its discriminative ability in distinguishing different brains. We examined the correlations between symptom alleviation and indicators calculated from the amplitude and FS obtained through band-pass filtering and the AFS, and we assessed the improvement achieved using the AFS in a paired T-test. The superiority of the AFS was quantified as an increase in distinguishability relative to that of the amplitude obtained through band-pass filtering (for a sample size of 32, with two abnormal samples removed).

In examining the adoption of the AFS quantification and peak frequency power on the medication set, we analysed the correlations (sample size of 32, with two abnormal samples removed) with symptom alleviation in 100 subsamples. In general, the sensitivity of AFS quantification to the peak frequency drift may be reflected by comparing the correlation proportions in all of the subsamples with the peak frequency power itself. Furthermore, we conducted a paired T-test (sample size of 100) between the AFS and peak frequency power to examine the r values in the correlations with symptom alleviation.

On the DBS dataset, we conducted a paired T-test to compare the abilities of the AFS, amplitude, and FS obtained through band-pass filtering in distinguishing conditions.

The statistical analyses were conducted using custom scripts in MATLAB. The alleviation of clinical symptoms was assessed using the UPDRS part III score, which is denoted as UPDRS OFF–ON. Correlations were examined using Pearson's correlation coefficient (R^2) because of the linear correlation coefficient for each hemisphere. The significance of the correlations was expressed as 95% confidence intervals calculated through linear regression. To control for multiple comparisons in one figure, we applied the false discovery rate (FDR) correction procedure, which controls for the expected proportion of falsely rejected hypotheses [37]. Considering the small sample numbers, Wilcoxon rank-sum tests were conducted as paired sample tests. In this paper, all of the data are given as the mean ± standard deviation unless mentioned otherwise.

Results

Changes in the instantaneous amplitude and FS captured by the AFS

In real recordings, the instantaneous amplitude and instantaneous frequency are correlated and usually vary concurrently, making it difficult to establish whether the AFS captures changes in both. This section considers simulated oscillations in the low-beta band. The two simulated signals were generated from the same real signal, and we independently simulated the instantaneous amplitude n and the FS k on them. The time-frequency spectra provided us with an overview of these changes (Fig. 2AD). The offline Hilbert transform was subsequently used

to extract the instantaneous amplitude and instantaneous frequency of the two simulated signals (Fig. 2BE).

AFS and amplitude based on band-pass filtering identified the amplitude change in the simulated signal with similar performance, as shown in Table 2 and Fig. 2C. In contrast, the amplitude obtained through band-pass filtering was limited in terms of detecting changes in FS, whereas the AFS had high sensitivity to variations in the FS (Fig. 2F). The variances in indicators for different parameter settings, quantified by the KLD, are presented in Table 2. A higher KLD for the AFS indicates the superiority of the AFS in discriminating parameter changes in the simulated signal. In terms of the correlation between the parameter sequence and the two indicators, Table 2 shows that only the AFS was significantly correlated ($R^2 = 0.524, p = 0$) with the change in FS.
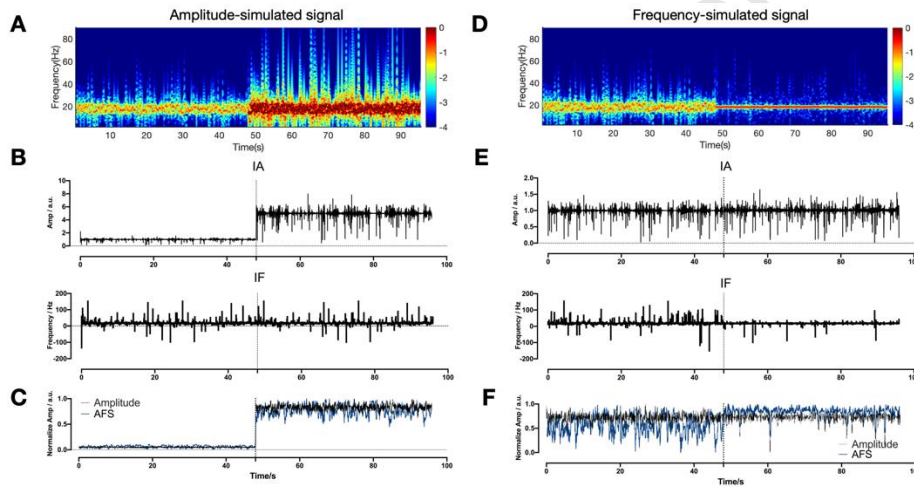

Figure 2: AFS effectively capturing both the amplitude and FS. (A) and (D) depict the power spectra of the simulated signals for the two tests. There are increases in the amplitude alone (A) and FS only (D) at 48 s. The top and bottom graphs in (B) and (E) show the results of the offline Hilbert transform for the instantaneous amplitude (IA) and instantaneous frequency (IF). (C) and (F) compare the results for the amplitude based on band-pass filtering (black lines) and the AFS (blue lines).

	Amplitude based on band-pass filter	AFS
Amplitude simulation		
Correlation (R^2)	0.992	0.958
KLD	32.24	49.77
FS simulation		
Correlation (R^2)	0.00062	0.524
KLD	0.198	12.24

Table 2: Ability of the indicators to capture amplitude and FS changes. The R^2 value represents the correlation between the amplitude parameter $\boldsymbol{n}$ / FS parameter $\boldsymbol{k}$ and the amplitude based on band-pass filtering or the AFS. Together with the KLD between the indicators before and after

simulation, the results imply that both indicators can differentiate the amplitude-simulated signal but only the AFS can distinguish the FS-simulated signal.

Better correlation of AFS quantification with symptom alleviation

As previously mentioned, in real LFP recordings, the amplitude and FS might change at the same time [4], [8], [18], [35]. It was found that the AFS was highly correlated with the amplitude obtained through band-pass filtering (Fig. 3A). However, the amplitude may not reflect changes in FS, in which case the AFS quantification is superior (Fig. 3A, grey area). In this section, we explore whether these additional frequency stabilities might allow the AFS to reflect more pathological information.

The ability of the AFS to follow the amplitude and FS were first investigated for real recordings. Among the complete dataset, the mean value of AFS correlated with the amplitude ($R^2 = 0.997, p < 0.0001$; Fig. 3 B i) and FS ($R^2 = 0.278, p < 0.0001$; Fig. 3 B ii) based on the band-pass filtering of low-beta oscillation.

We then examined the AFS, amplitude, and FS obtained through band-pass filtering and their differences between ON and OFF levodopa conditions ($KLD\ OFF-ON$). In general, AFS had greater distinguishability ($KLD = 13.68 \pm 16.43$) than the amplitude ($KLD = 11.05 \pm 14.60$) and FS ($KLD = 1.16 \pm 2.42$) based on band-pass filtering across both hemispheres (Fig. 1C). Furthermore, across both hemispheres, the KLD of AFS correlated with symptom alleviation ($R^2 = 0.229, p = 0.0137$; Fig. 3D). However, the KLD of the low-beta amplitude was not significantly correlated with symptom alleviation ($R^2 = 0.0645, p = 0.1606$; Fig. 3 Ci) or FS ($R^2 = 0.0836, p = 0.1933$; Fig. 3 Cii). Beyond the low-beta band, we extended the analysis to other frequency bands, such as theta (3-6 Hz), alpha (6-12 Hz), high-beta and low-gamma (24-48 Hz), and high-gamma (48-96 Hz) bands, as shown in the Supplementary Materials (Supplementary Fig. 4). However, we did not observe correlations between clinical scores and either changes in amplitude or changes in AFS in these bands.

We found that the medication distinguishability was significantly higher for the AFS than for the amplitude ($Cohen's\ D = 0.23878, p = 0.0175$; Fig. 3 F) or FS ($Cohen's\ D = 1.0195, p < 0.0001$; Fig. 3 F) only. However, increases in the amplitude did not correlate with symptom alleviation ($R^2 = 0.0325, p = 0.3236$; Fig. 3 Fi), and neither did increases in FS ($R^2 = 0.0628, p = 0.1667$; Fig. 3 Fii), suggesting that it was not a simple combination of amplitude and FS that drove the correlation between the AFS and motor symptoms of PD. The results obtained for different window lengths confirmed that the correlation between the AFS and symptom alleviation was in general better than that between the amplitude based on band-pass filtering and symptom alleviation.
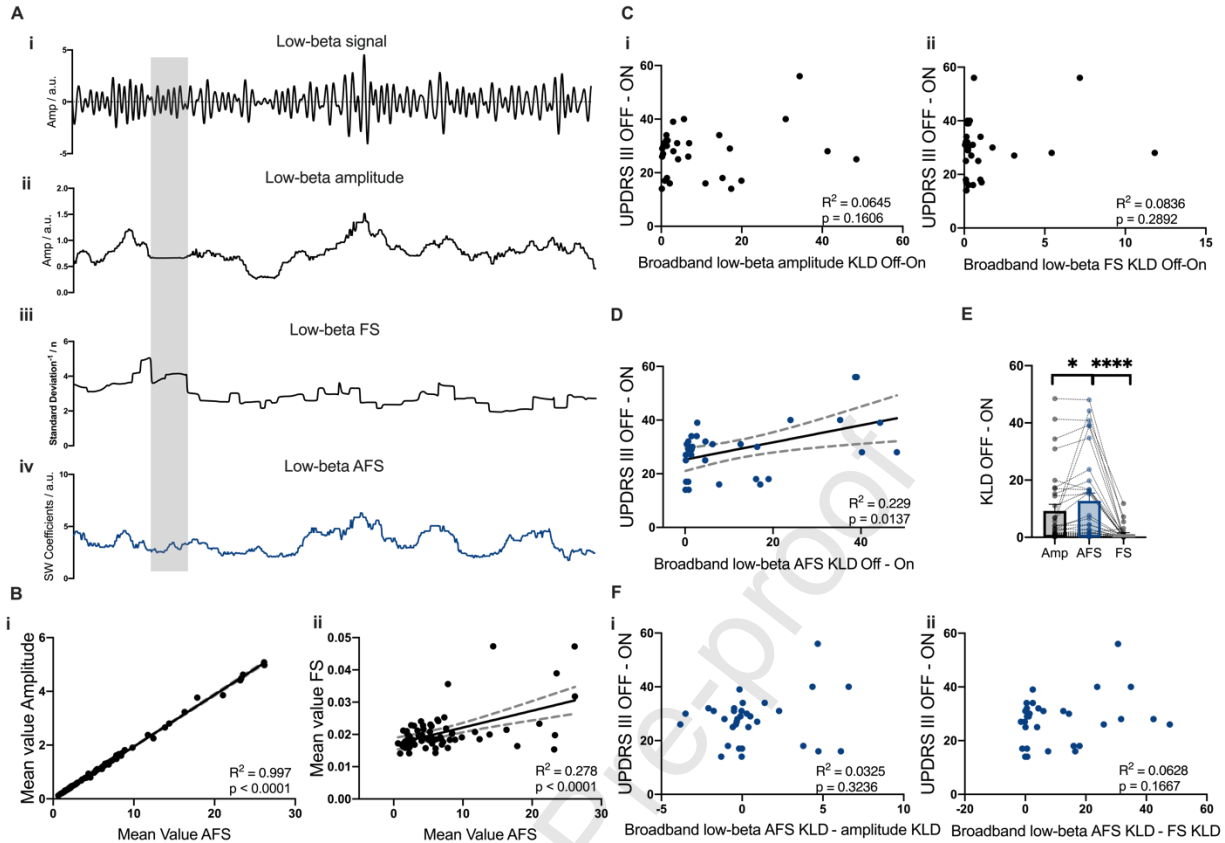
Figure 3: AFS quantification having better correlation than amplitude or FS based on band-pass filtering with symptom alleviation. (A) (i) Low-beta signal from the band-pass filter. (ii) Low-beta amplitude based on band-pass filtering. (iii) Low-beta FS based on band-pass filtering. (iv) Low-beta AFS from stationary wavelet (SW) coefficients. The grey area highlights where the signal has a different FS that cannot be captured by the amplitude based on band-pass filtering but is indicated in the quantification. (B) Ability of the AFS to follow the amplitude and FS in real recordings. In all recordings within the medication dataset, the mean value of the AFS correlated with the mean value of the amplitude ($R^2 = 0.997, p < 0.0001$) and FS ($R^2 = 0.278, p < 0.0001$) based on band-pass filtering. (C) (i) The distinguishability of amplitude based on band-pass filtering ($R^2 = 0.0645, p = 0.1606$) did not show such a correlation. (ii) The distinguishability of the FS based on band-pass filtering also did not show such a correlation ($R^2 = 0.0836, p = 0.2892$). (D) The ability to distinguish between different conditions in AFS was correlated ($R^2 = 0.229, p = 0.0137$) with symptom alleviation. (E) AFS showed higher distinguishability than the amplitude ($Cohen's\ D = 0.23878, p = 0.0175$) or FS ($Cohen's\ D = 1.0195, p < 0.0001$) based on band-pass filtering only on the medication dataset. (F) Increases in distinguishability from the amplitude based on band-pass filtering to the AFS did not correlate ($R^2 = 0.0325, p = 0.3236$) with symptom alleviation, and increases from FS showed no correlation ($R^2 = 0.0628, p = 0.1667$). All of the correlations were corrected using the FDR.

AFS insensitivity to peak frequency changes

In the context of PD, studies have mostly focused on the relationship between symptom alleviation and peak beta power rather than broadband beta power [7]–[9], [11]. As shown by previous studies and our results, if the individual peak frequency band is considered, the power of peak low-beta oscillation correlates with symptom alleviation ($R^2 = 0.221, p = 0.0374$; Fig. 4A) [7]. To achieve this result, the peak frequency was first identified in the average PSD in the low-beta frequency range. The peak low-beta power was calculated with a 5-Hz frequency band around the peak frequency and then correlated with UPDRS OFF–ON.

Nevertheless, the peak frequency might vary across time (Fig. 4B; the peak frequency drift is visualised from the peak frequency of the PSD in the 2-s sliding window with a step of 0.5 s), and more than one peak might exist in the beta band in the PSD in some cases [16]. The peak frequency power limited by a narrow band failed to identify and track such variations. When using stationary wavelets to quantify the AFS as we propose, there is no need to select the individual peak frequency. Instead, the fourth-layer stationary wavelet coefficients were selected as the broadband for all patients in the AFS. This approach may be less susceptible to peak frequency drifts because it covers a wider frequency range.

To investigate the sensitivity of the AFS to peak frequency changes, we calculated the correlation proportions defined in the Methods section. In a segment session, 100 sub-datasets were generated. We found that 66% of the subsampled data revealed a significant correlation between an AFS change and symptom alleviation. However, only 33% of the subsamples showed a significant correlation between a change in the peak frequency power and symptom alleviation. Furthermore, r values obtained using the AFS were significantly higher than those obtained using the peak frequency power
($0.388 \pm 0.082 (AFS)$ $vs.$ $0.309 \pm 0.076 (Peak\ PSD)$, $Cohen's\ D = 0.502, p < 0.0001$; Fig. 4C). Likewise, for other segment lengths, changes in the AFS were superior in characterising medication-induced differences (Supplementary Fig. 5B).

To determine the cause of the discrepancy between the peak power marker and the AFS marker, we selected the subsample that had the most difference among the 100 sub-datasets. The AFS marker correlated with symptom alleviation ($R^2 = 0.182, p = 0.0296$; Fig. 4 D), whereas the peak frequency did not ($R^2 = 0.0338, p = 0.3141$; Fig. 4 D). At the individual level, the peak frequency was less effective at representing changes due to its narrow frequency range. This is evident in cases in which several peaks existed within the beta band and peak power failed to follow the changes effectively, but the AFS difference remained clear ($peak\ PSD\ Off - On$, $AFS\ KLD = 20.0925$; Fig. 4E). This suggests that the AFS is insensitive to drifts in the peak frequency as long as they fall in a broad range (12–24 Hz in this study).
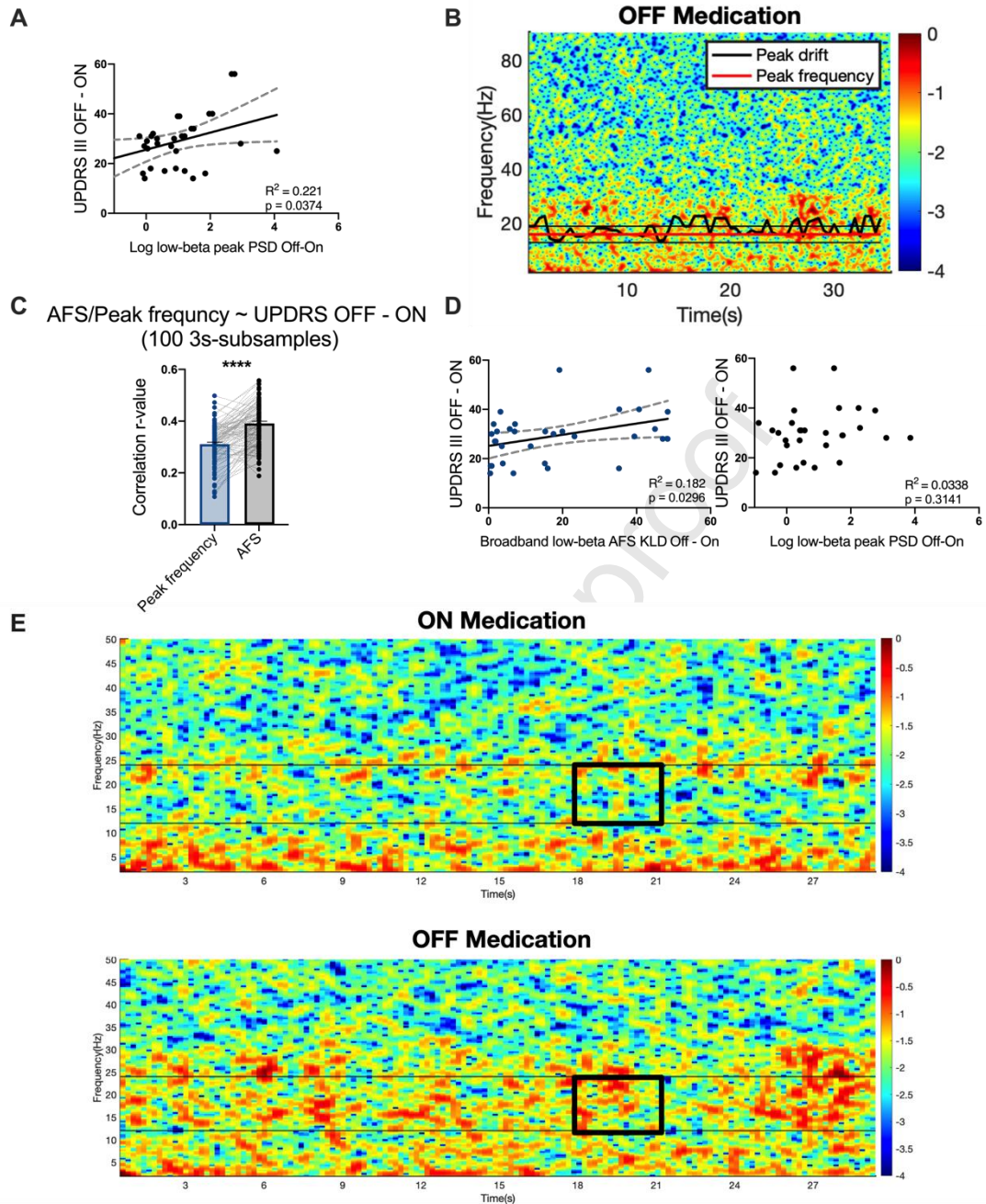
Figure 4: AFS insensitivity to peak frequency changes. (A) Overall, the peak low-beta power changes in the low-beta band exhibited a clear correlation with symptom alleviation ($R^2 = 0.221, p = 0.0320$). (B) The peak frequency (thick red line) was defined in the PSD from the whole data set and normally within a range of ± 2 Hz (thin black lines). However, the peak frequency varies across time, which is the peak drift (thick black line), and it can be beyond the peak frequency band. (C) By segmenting signals into shorter fragments (3 s), we generated 100 subsets of signals for all hemispheres. Among these 100 subsamples, the correlation with symptom alleviation indicated by r values shows an improvement ($Cohen's\ D = 0.502, p < 0.0001$) from the peak frequency power (0.388 ± 0.082) to the AFS (0.309 ± 0.076). (D) One case in the subsample is presented to illustrate why a greater correlation with the AFS was

detected in the datasets. In this case, the peak frequency power (right) was not correlated ($R^2 = 0.0338, p = 0.3141$), whereas the AFS showed a clinically correlated difference between OFF and ON medications ($R^2 = 0.182, p = 0.0296$). (E) For one subject in the case of (D), in the spectrum for one hemisphere, there were multiple peaks in the band (black square), and the peak power failed to capture the differences ($peak\ PSD\ Off - On = 0.4527$); however, the AFS quantification difference was clear ($AFS\ KLD = 20.0925$). All of the correlations were corrected using the FDR.

Better distinguishability of stimulation effects through AFS quantification than through amplitude or FS quantification

In this section, we examine the abilities of the different quantifications to distinguish ON/OFF stimulation conditions (Fig. 5A). The AFS ($KLD = 10.00 \pm 14.72$) had greater distinguishability ($Cohen's\ D = 0.104, p = 0.0061; Cohen's\ D = 0.805, p < 0.0001$; Fig. 5B) than the amplitude ($KLD = 8.34 \pm 13.56$) and FS ($KLD = 0.939 \pm 3.25$) based on band-pass filtering.
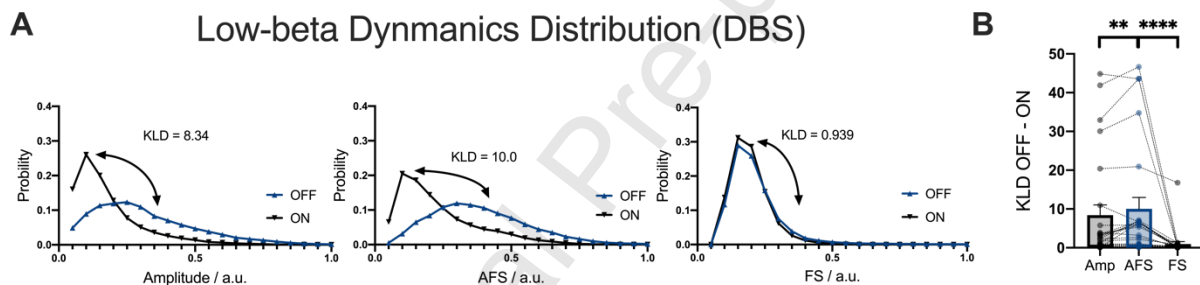

Figure 5: AFS in the stimulation set. (A) The KLD serves as a measurement of pairwise differences. The distributions of the indicator AFS (middle), amplitude (left), and FS (right) based on band-pass filtering are provided for ON/OFF stimulation conditions, with the results serving as an illustrative example of the visualisation of distributions averaged across all patients. To account for participant-specific differences, all of the indicators were standardised to the range [0,1] and displayed in hemisphere units for visual representation. (B) The AFS was more effective than the amplitude ($Cohen's\ D = 0.104, p = 0.0061$) and FS ($Cohen's\ D = 0.805, p < 0.0001$) from band-pass filtering in distinguishing the stimulation effect.

Discussion

Our findings suggest that the AFS excels in capturing joint information from the amplitude and FS within signals, surpassing the capabilities of measurements based on the amplitude or FS of low-beta alone. In addition, the AFS quantification showed more robust effects of medication and DBS treatment. Furthermore, the AFS may be useful in decoding other signals that contain distinct oscillations, such as tremor-band oscillations (4 to 10 Hz, thalamic ventral intermediate nucleus) in patients suffering essential tremor [36] and theta oscillations (3 to 6 Hz, globus pallidus internus) in patients suffering dystonia [37].

Superiority of AFS

Both the amplitude and frequency provide valuable information for understanding the pathophysiological characteristics of neural activities. The strength of AFS resides in its capacity to provide joint information on the amplitude and FS, as we showed first for simulation data and then for medication and stimulation effects in real patient data. The rationale behind the superiority of the AFS, relative to the amplitude or FS alone, is as follows. AFS quantification based on stationary wavelet coefficients was developed in the 1980s [38] and was shown to have potential in the analysis of periodic neural indicators [39]. As both the amplitude and FS have an inverse relationship with medication in PD [4], the selection of the mother wavelet function [27], [40], resembling a 'sinc' function (refer to Supplementary Fig. 1A), is important, where higher FS (resulting in waveforms resembling a perfect sine wave) and a higher amplitude correspond to greater wavelet coefficients. In addition, AFS quantification takes the median value of stationary wavelet coefficients, which is the optimal value with which to represent randomness in a signal [28]. The AFS is thus supposed to be more robust than simple smoothing against noise. In addition, there is no need to pre-select the peak frequency; instead, the determination of frequency bands relies on the inherent configuration, including the sampling frequency and number of layers, of the transform.

Condition differences in the AFS

Distinguishability is represented by the KLD, which is a non-negative metric [41]. The KLD is zero when two conditions (or distributions) are identical. The KLD of the amplitude based on band-pass filtering has a value of 0.1911 (i.e., a value near zero) before and after the FS simulation, whereas the KLD of the AFS is much larger than zero. We thus posit that the AFS contains frequency variations in the simulated signal that cannot be solely attributed to changes in amplitude. The present simulation experiment validated our hypothesis that the AFS captures fluctuations in both amplitude and FS.

In complex systems that involve oscillator interactions, amplitude and frequency variations are mathematically associated [18], [42], [43]. Nevertheless, it is worth noting that frequency changes in real recordings do not consistently align with changes in amplitude, as demonstrated by the occurrence of the phase slip [4], [44]. In real records, information on the FS can still be used to decode motor functions. Figure 3E illustrates that the KLDs of medication ON vs. OFF and stimulus ON vs. OFF for the AFS are much greater than those for the amplitude based on band-pass filtering or the FS. This highlights the importance of considering joint information [42], [44], [45]. KLDs of the AFS in the medication dataset correlated with symptom alleviation, implying that KLDs capture more information for the decoding of motor functions. However, the better performance of the AFS relative to the amplitude and FS was not significantly associated with symptom relief. This indicates that the AFS is not only a linear combination of these two components but involves a non-linear function. In addition, there may be an interaction between the amplitude and FS during oscillations. Pathological investigations into Parkinson's disease have demonstrated that amplitude fluctuations might be affected by the resonance function between the STN and the ventral lateral thalamic network [46] and could be modulated by the stimulation at specific phases [47], [48].

Nevertheless, it is important to recognise that the KLD level differs among individual patients. One possible explanation is that each patient has his or her own induced beta reduction effects. In addition, while the two distributions had a consistent bin size of 20 in the present study, they differed in terms of the bin range. Given the comparable tendencies identified in the AFS (i.e., amplitude, frequency, and symmetry) in the KLD, we hypothesise that the changes observed relate to the effects of medications or stimulation. Nevertheless, there is still debate over the suitable range for segmentation.

AFS and peak frequency drift

Considerable attention has been devoted to investigating the importance of peak beta power as an indicator of parkinsonian symptoms [7], [8], [11], [12]. However, certain questions persist. First, some patients may exhibit more than one peak in a plot of the power spectra density, and the peak frequency may drift over time [16]. In addition, a wide bandwidth of the pathological oscillation peak frequency might result in more noise from other frequency bands. In contrast, a narrow bandwidth may fail to capture drifts in the peak frequency as we showed in Fig. 4B. These peak frequency drifts may be caused by resonance between coupled oscillators [49], which implies neurons are synchronised yet have different matching frequencies. Although the methods for quantifying these drifts and the mechanisms underlying the drifts require additional investigation, we hypothesised that peak frequency drifts are reflected in FS changes. In light of these considerations, we found that peak frequency drifts may be misleading when assessing the association between the peak frequency power and symptom alleviation. As the AFS can capture FS over a broad frequency range, it is insensitive to peak frequency drifts.

Implications for adaptive DBS

Beta activity has emerged as a highly suitable feedback signal for adaptive DBS because of its demonstrated clinical relevance and consistency [50]. In addition, phase-dependent control has shown potential in precise neuromodulation [44], [47], [51], [52]. FS information is less combined with power-based control [4] and is thus important to AFS quantification. As the SWT can be used in real-time implementation and considering FS within a signal, the adoption of quantification in adaptive DBS strategies is a flexible and adaptable approach that can potentially enhance the precision and efficacy of DBS interventions.

Limitations

The proposed method is based on the implementation of the SWT through the cascading of low-pass and high-pass filters. Its online application has been highlighted. It is noted that the determination of frequency bands relies on the inherent configuration of the transform. Considering that these bands are defined in part by the sampling rate, their range is constrained. Consequently, here, we only compared broadband signals in an amplitude-based method and AFS quantification. However, the superiority of FS with respect to the amplitude based on band-pass filtering of the peak beta frequency requires exploration. The main issue is that a narrow-

band signal has fewer frequency components, and the instantaneous FS might contain less state-dependent information.

An additional limitation of our study is that the AFS was not studied on a daily living dataset including movement. A potential feedback signal in DBS should be immune to movement-related noise. In terms of methodology, we have incorporated a control chart approach into our algorithm to increase its robustness against noise. Further study on free-leaving data is expected to provide further insights.

Conclusions

In this study, we presented an AFS metric for combining amplitude and FS information. We showed that the broadband AFS can track changes in amplitude and FS, resulting in additional pathogenic information on medication or stimulation conditions, through simulation and the analysis of real recordings. Furthermore, even considering the beta peak power, the AFS is unaffected by peak drifts and maintains a link with motor performance. The AFS warrants further study to assess whether it can be quantified on a daily living dataset and help decode pathophysiological neural activities related to motor functions in the LFPs of a patient with PD.

Acknowledgements

References

[1]   P. Brown and D. Williams, "Basal ganglia local field potential activity: Character and functional significance in the human," *Clin. Neurophysiol.*, vol. 116, no. 11, pp. 2510–2519, 2005, doi: 10.1016/j.clinph.2005.05.009.

[2]   G. Buzsáki, C. A. Anastassiou, and C. Koch, "The origin of extracellular fields and currents-EEG, ECoG, LFP and spikes," *Nat. Rev. Neurosci.*, vol. 13, no. 6, pp. 407–420, 2012, doi: 10.1038/nrn3241.

[3]   G. Buzsáki, "Neural Syntax: Cell Assemblies, Synapsembles, and Readers," *Neuron*, vol. 68, no. 3, pp. 362–385, 2010, doi: 10.1016/j.neuron.2010.09.023.

[4]   A. Averna, S. Marceglia, A. Priori, and G. Foffani, "Amplitude and frequency modulation of subthalamic beta oscillations jointly encode the dopaminergic state in Parkinson's disease," *npj Park. Dis.*, vol. 8, no. 1, 2022, doi: 10.1038/s41531-022-00399-4.

[5]   S. Little and P. Brown, "The functional role of beta oscillations in Parkinson's disease," *Park. Relat. Disord.*, vol. 20, no. SUPPL.1, pp. S44–S48, 2014, doi: 10.1016/S1353-8020(13)70013-0.

[6]   A. A. Kühn *et al.*, "Pathological synchronisation in the subthalamic nucleus of patients with Parkinson's disease relates to both bradykinesia and rigidity," *Exp. Neurol.*, vol. 215, no. 2, pp. 380–387, 2009, doi: 10.1016/j.expneurol.2008.11.008.

[7]   A. A. Kühn, A. Kupsch, G. H. Schneider, and P. Brown, "Reduction in subthalamic 8-35 Hz oscillatory activity correlates with clinical improvement in Parkinson's disease," *Eur. J. Neurosci.*, vol. 23, no. 7, pp. 1956–1960, 2006, doi: 10.1111/j.1460-9568.2006.04717.x.

[8]   G. Tinkhauser, A. Pogosyan, H. Tan, D. M. Herz, A. A. Kühn, and P. Brown, "Beta burst dynamics in Parkinson's disease off and on dopaminergic medication," *Brain*, vol. 140, no. 11, pp. 2968–2981, 2017, doi: 10.1093/brain/awx252.

[9]   R. Lofredi *et al.*, "Subthalamic beta bursts correlate with dopamine-dependent motor symptoms in 106 Parkinson's patients," *npj Park. Dis.*, vol. 9, no. 1, pp. 1–9, 2023, doi: 10.1038/s41531-022-00443-3.

[10]   W. Bouthour, P. Mégevand, J. Donoghue, C. Lüscher, N. Birbaumer, and P. Krack, "Biomarkers for closed-loop deep brain stimulation in Parkinson disease and beyond," *Nat. Rev. Neurol.*, vol. 15, no. 6, pp. 343–352, 2019, doi: 10.1038/s41582-019-0166-4.

[11]   G. Tinkhauser *et al.*, "The modulatory effect of adaptive deep brain stimulation on beta bursts in Parkinson's disease," *Brain*, vol. 140, no. 4, pp. 1053–1067, 2017, doi: 10.1093/brain/awx010.

[12]   S. Little *et al.*, "Adaptive deep brain stimulation in advanced Parkinson disease.," *Ann. Neurol.*, vol. 74, no. 3, pp. 449–457, 2013, doi: 10.1002/ana.23951.

[13]   S. Little *et al.*, "Bilateral adaptive deep brain stimulation is effective in Parkinson's disease," *J. Neurol. Neurosurg. Psychiatry*, vol. 87, no. 7, pp. 717–721, 2016, doi: 10.1136/jnnp-2015-310972.

[14]   S. He *et al.*, "Beta-triggered adaptive deep brain stimulation during reaching movement in Parkinson's disease," *Brain*, vol. 146, no. 12, pp. 5015–5030, 2023, doi: 10.1093/brain/awad233.

[15]   S. He *et al.*, "Subthalamic beta-targeted neurofeedback speeds up movement initiation but increases tremor in parkinsonian patients," *Elife*, vol. 9, pp. 1–20, 2020, doi: 10.7554/eLife.60979.

[16]   N. Darcy *et al.*, "Spectral and spatial distribution of subthalamic beta peak activity in

Parkinson's disease patients," *Exp. Neurol.*, vol. 356, no. May, p. 114150, 2022, doi: 10.1016/j.expneurol.2022.114150.

[17] S. L. Schmidt, J. J. Peters, D. A. Turner, and W. M. Grill, "Continuous deep brain stimulation of the subthalamic nucleus may not modulate beta bursts in patients with Parkinson's disease," *Brain Stimul.*, vol. 13, no. 2, pp. 433–443, 2020, doi: 10.1016/j.brs.2019.12.008.

[18] C. H. Yeh *et al.*, "Waveform changes with the evolution of beta bursts in the human subthalamic nucleus," *Clin. Neurophysiol.*, vol. 131, no. 9, pp. 2086–2099, 2020, doi: 10.1016/j.clinph.2020.05.035.

[19] Maiti and Bidinger, *Wavelet and Statistics*, vol. 53, no. 9. 1981.

[20] Y. Nie *et al.*, "Subthalamic dynamic neural states correlate with motor symptoms in Parkinson's Disease," *Clin. Neurophysiol.*, vol. 132, no. 11, pp. 2789–2797, 2021, doi: 10.1016/j.clinph.2021.07.022.

[21] S. Khawaldeh *et al.*, "Balance between competing spectral states in subthalamic nucleus is linked to motor impairment in Parkinson's disease," *Brain*, vol. 145, no. 1, pp. 237–250, 2022, doi: 10.1093/brain/awab264.

[22] C. Wiest *et al.*, "Local field potential activity dynamics in response to deep brain stimulation of the subthalamic nucleus in Parkinson's disease," *Neurobiol. Dis.*, vol. 143, no. June, 2020, doi: 10.1016/j.nbd.2020.105019.

[23] C. Wiest *et al.*, "Subthalamic deep brain stimulation induces finely-tuned gamma oscillations in the absence of levodopa," *Neurobiol. Dis.*, vol. 152, no. December 2020, 2021, doi: 10.1016/j.nbd.2021.105287.

[24] C. Wiest *et al.*, "The aperiodic exponent of subthalamic field potentials reflects excitation/inhibition balance in Parkinsonism," *Elife*, vol. 12, pp. 1–19, 2023, doi: 10.7554/eLife.82467.

[25] M. S. Fabus, A. J. Quinn, C. E. Warnaby, and M. W. Woolrich, "Automatic decomposition of electrophysiological data into distinct nonsinusoidal oscillatory modes," *J. Neurophysiol.*, vol. 126, no. 5, pp. 1670–1684, 2021, doi: 10.1152/jn.00315.2021.

[26] Y. Nie *et al.*, "Subthalamic dynamic neural states correlate with motor symptoms in Parkinson's Disease," *Clin. Neurophysiol.*, vol. 132, no. 11, pp. 2789–2797, 2021, doi: 10.1016/j.clinph.2021.07.022.

[27] H. Luo *et al.*, "Dynamic Neural State Identification in Deep Brain Local Field Potentials of Neuropathic Pain," *Front. Neurosci.*, vol. 12, p. 237, 2018, doi: 10.3389/fnins.2018.00237.

[28] D. L. Donoho and I. M. Johnstone, "Minimax estimation via wavelet shrinkage," *Ann. Stat.*, vol. 26, no. 3, pp. 879–921, 1998, doi: 10.1214/aos/1024691081.

[29] D. L. Donoho, "De-Noising by Soft-Thresholding," vol. 41, no. 3, 1995.

[30] D. L. Donoho and I. M. Johnstone, "Adapting to unknown smoothness via wavelet shrinkage," *J. Am. Stat. Assoc.*, vol. 90, no. 432, pp. 1200–1224, 1995, doi: 10.1080/01621459.1995.10476626.

[31] G. Baldazzi *et al.*, "Systematic analysis of wavelet denoising methods for neural signal processing," *J. Neural Eng.*, vol. 17, no. 6, p. 66016, 2020, doi: 10.1088/1741-2552/ABC741.

[32] L. Debnath and F. A. Shah, *Wavelet transforms and their applications, second edition*. 2015.

[33] M. N. Do and M. Vetterli, "Wavelet-based texture retrieval using generalized Gaussian

density and Kullback-Leibler distance," *IEEE Trans. Image Process.*, vol. 11, no. 2, pp. 146–158, 2002, doi: 10.1109/83.982822.

[34] E. Lowet, M. J. Roberts, A. Peter, B. Gips, and P. De Weerd, "A quantitative theory of gamma synchronization in macaque V1," *Elife*, vol. 6, pp. 1–44, 2017, doi: 10.7554/eLife.26642.

[35] A. K. Engel *et al.*, "Beta band stability over time correlates with Parkinsonian rigidity and bradykinesia," *Trends Neurosci.*, vol. 12, no. 2, pp. 383–388, 2018, doi: 10.1016/S1364-6613(00)01568-0.

[36] M. Scherer *et al.*, "Single-neuron bursts encode pathological oscillations in subcortical nuclei of patients with Parkinson's disease and essential tremor," *Proc. Natl. Acad. Sci. U. S. A.*, vol. 119, no. 35, 2022, doi: 10.1073/pnas.2205881119.

[37] R. Zhang, Y. Nie, W. Dai, S. Wang, and X. Geng, "Balance between pallidal neural oscillations correlated with dystonic activity and severity," *Neurobiol. Dis.*, vol. 183, no. May, p. 106178, 2023, doi: 10.1016/j.nbd.2023.106178.

[38] I. Daubechies, "Wavelets and applications," *Princet. Companion to Math.*, pp. 848–862, 2010, doi: 10.1121/1.404335.

[39] A. N. Pavlov, A. E. Hramov, A. A. Koronovskii, E. Y. Sitnikova, V. A. Makarov, and A. A. Ovchinnikov, "Wavelet analysis in neurodynamics," *Physics-Uspekhi*, vol. 55, no. 9, pp. 845–875, 2012, doi: 10.3367/ufne.0182.201209a.0905.

[40] Y. Nie *et al.*, "Subthalamic dynamic neural states correlate with motor symptoms in Parkinson's Disease," *Clin. Neurophysiol.*, vol. 132, no. 11, pp. 2789–2797, 2021, doi: https://doi.org/10.1016/j.clinph.2021.07.022.

[41] M. Broniatowski, "ESTIMATION OF THE KULLBACK-LEIBLER To cite this version : HAL Id : hal-04363067," 2023.

[42] S. Nelli, S. Itthipuripat, R. Srinivasan, and J. T. Serences, "Fluctuations in instantaneous frequency predict alpha amplitude during visual perception," *Nat. Commun.*, vol. 8, no. 1, 2017, doi: 10.1038/s41467-017-02176-x.

[43] T. T. K. Munia and S. Aviyente, "Time-Frequency Based Phase-Amplitude Coupling Measure For Neuronal Oscillations," *Sci. Rep.*, vol. 9, no. 1, pp. 1–15, 2019, doi: 10.1038/s41598-019-48870-2.

[44] H. Cagnan, E. P. Duff, and P. Brown, "The relative phases of basal ganglia activities dynamically shape effective connectivity in Parkinson's disease," *Brain*, vol. 138, no. 6, pp. 1667–1678, 2015, doi: 10.1093/brain/awv093.

[45] D. Spampinato, E. Avci, J. Rothwell, and L. Rocchi, "Frequency-dependent modulation of cerebellar excitability during the application of non-invasive alternating current stimulation," *Brain Stimul.*, vol. 14, no. 2, pp. 277–283, Mar. 2021, doi: 10.1016/j.brs.2021.01.007.

[46] H. Cagnan *et al.*, "The nature of tremor circuits in parkinsonian and essential tremor," *Brain*, vol. 137, no. 12, pp. 3223–3234, 2014, doi: 10.1093/brain/awu250.

[47] A. B. Holt *et al.*, "Phase-dependent suppression of beta oscillations in parkinson's disease patients," *J. Neurosci.*, vol. 39, no. 6, pp. 1119–1134, 2019, doi: 10.1523/JNEUROSCI.1913-18.2018.

[48] C. G. McNamara, M. Rothwell, and A. Sharott, "Stable, interactive modulation of neuronal oscillations produced through brain-machine equilibrium," *Cell Rep.*, vol. 41, no. 6, p. 111616, 2022, doi: 10.1016/j.celrep.2022.111616.

[49] Y. Chen, J. Wang, Y. Kang, and M. B. Ghori, "Emergence of beta oscillations of a

resonance model for Parkinson's disease," *Neural Plast.*, vol. 2020, 2020, doi: 10.1155/2020/8824760.

[50]   Z. Yin *et al.*, "Local field potentials in Parkinson's disease: A frequency-based review," *Neurobiol. Dis.*, vol. 155, p. 105372, 2021, doi: 10.1016/j.nbd.2021.105372.

[51]   J. Fell and N. Axmacher, "The role of phase synchronization in memory processes," *Nat. Rev. Neurosci. 2011 122*, vol. 12, no. 2, pp. 105–118, 2011, doi: 10.1038/nrn2979.

[52]   E. Lowet, M. Roberts, A. Hadjipapas, A. Peter, J. van der Eerden, and P. De Weerd, "Input-Dependent Frequency Modulation of Cortical Gamma Oscillations Shapes Spatial Synchronization and Enables Phase Coding," *PLoS Comput. Biol.*, vol. 11, no. 2, pp. 1–44, 2015, doi: 10.1371/journal.pcbi.1004072.

Highlights:

- The new quantification amplitude and frequency stability (AFS) comprehensively captures variations in the amplitude and frequency stability of broad band subthalamic nucleus beta oscillations.
- AFS quantification indicates better correlation than amplitude or frequency stability based on band-pass filtering with symptom alleviation.
- AFS can be implemented in real-time for adaptive deep brain stimulation.